



An Intermediate-Temperature Oxygen Transport Membrane Based on Rare-Earth Doped Bismuth Oxide $\text{Dy}_{0.08}\text{W}_{0.04}\text{Bi}_{0.88}\text{O}_{2-8}$

Tao Hong,^a Shuming Fang,^b Mingyang Zhao,^a Fanglin Chen,^c Hailiang Zhang,^b Siwei Wang,^b and Kyle S. Brinkman^{a,z}

^aDepartment of Materials Science and Engineering, Clemson University, Clemson, South Carolina 29634, USA

^bNanowise LLC, Lexington, Kentucky 40513, USA

^cDepartment of Mechanical Engineering, University of South Carolina, Columbia, South Carolina 29208, USA

In this work, a ceramic oxygen pump based on dysprosium and tungsten co-doped bismuth oxide (DWSB) was synthesized and characterized. The DWSB oxygen ion conducting electrolyte with a composition of $\text{Dy}_{0.08}\text{W}_{0.04}\text{Bi}_{0.88}\text{O}_{2-8}$ displayed the highest oxygen ion conductivity and was chemically compatible with the $\text{La}_{0.8}\text{Sr}_{0.2}\text{MnO}_{3-\delta}$ (LSM) electrode material. A composite electrode was fabricated with DWSB-LSM in the mass fraction of 50:50 exhibiting the lowest polarization resistance with the DWSB electrolyte. In the composite electrode, larger DWSB particles act as backbone for the oxygen transport pathway, while LSM particles deposited on the surface of the DWSB backbone serve as mixed ionic-electronic conductors accelerating surface oxygen exchange. An oxygen flux of $5.9 \text{ mL cm}^{-2} \text{ min}^{-1}$ at 650°C under 1 V applied bias was realized in the DWSB electrolyte (0.75 mm) supported membrane incorporating DWSB-LSM electrodes on feed and permeate sides. Further improvements to the electrochemical performance were achieved by fabricating a thin, electrode supported DWSB membrane ($\sim 12 \mu\text{m}$). The current density for the electrode-supported cell was 5.4 A cm^{-2} under 2 V applied bias at 650°C which corresponds to an oxygen flux of $17 \text{ mL cm}^{-2} \text{ min}^{-1}$. Higher bias voltages were observed to accelerate the electrode reaction process leading to reduced polarization resistance that resulted in a remarkable growth of current density. This intelligent DWSB based oxygen pump is a promising materials system for high performance electrochemical oxygen separation.

© 2017 The Electrochemical Society. [DOI: 10.1149/2.1201704jes] All rights reserved.

Manuscript submitted December 22, 2016; revised manuscript received February 6, 2017. Published February 16, 2017.

A solid electrolyte oxygen separation (SEOS) device, also known as an oxygen pump, is an effective device to produce oxygen from air without using water.¹⁻³ Current systems based on high temperature oxygen ion conducting ceramic membranes work in two modes: i) chemical potential (oxygen partial pressure) driven flux where mixed ionic and electronic conductor (MIEC) materials are required and ii) oxygen pumps where an electrical potential is utilized to enact separation requiring only an oxygen ion conducting electrolyte.⁴ The advantages of ceramic oxygen membrane over other technologies for the oxygen pump systems are twofold: i) pure oxygen streams are produced and can then be combined with air to form varying levels of oxygen enriched gas; and ii) an oxygen transport membrane based on an oxygen pump is an electrochemical device, which enables continuous operation.

Oxide ionic conductors such as zirconia and ceria transport O^{2-} from the cathode to the anode side of the device when current is applied from an external power source.⁵ The current corresponds to an oxygen flux of $I/4F$ (where I is the current density, and F is the Faraday constant) moles per second transported through the solid electrolyte according to the Faraday's law. For example, an oxygen pump based on conventional yttrium doped zirconia (YSZ) electrolyte membrane needs to operate at 800°C which is provided by a high temperature furnace. Spirin et al.⁶ have designed an YSZ based device using a YSZ electrolyte ($170 \mu\text{m}$) with $\text{La}_{0.8}\text{Sr}_{0.2}\text{MnO}_{3-\delta}$ (LSM) electrodes ($20 \mu\text{m}$) based stack that was able to produce 150 ml min^{-1} pure oxygen with an applied power of 50 W at 800°C . Long term testing demonstrated a 83 ml min^{-1} oxygen flux rate with $<24 \text{ W}$ consumed power for 300 h. Conventional electrolyte materials such as YSZ have met the basic requirement of obtaining appreciable oxygen flux. However, the size of the devices is relatively large and the high operating temperature of 800°C requires a large amount of power. Although these materials may be sufficient for stationary applications, mobile applications including generating oxygen enriched gas in the field for medical relief efforts and military excursions require new materials systems that are more efficient and operate at lower temperature.

A new materials system consisting of oxide ion conducting materials that possess higher level of conductivity at much lower temperatures compared to that of YSZ at 800°C ($\sim 0.01 \text{ S cm}^{-1}$) and excellent electrolyte/electrode combinations is required to achieve

better performance.⁷ In addition, new manufacture techniques that enable the production of robust high surface area ceramic membranes that can be integrated into the devices are needed.⁸ Bismuth oxides, which have been stabilized through doping in the fluorite structure, have exceptionally high ionic conductivity and oxygen reduction reaction rates.⁹⁻¹² Takahashi et al. have identified two types of stabilized bismuth oxides: one is stabilized in a face-centered cubic (fcc) structure and the other in a rhombohedral structure.^{11,13,14} Both the cubic phase and the rhombohedral phase have high oxygen-ion conductivities because of numerous oxygen vacancies existing in the crystal structure. The selected dopants include the heavy rare-earth oxides Dy_2O_3 , Ho_2O_3 , Er_2O_3 , Tm_2O_3 , and Yb_2O_3 .¹¹ For example, the oxygen ion conductivity of 20 mol% erbia stabilized bismuth oxide (ESB) at 500°C (0.0268 Scm^{-1}) is 30 times greater than that of YSZ (0.0009 Scm^{-1}).¹¹ Moreover, bismuth oxides have a remarkably high oxygen surface exchange coefficient (k_{chem}), which is much higher (by a factor of 103 at 700°C) than that of YSZ and even competitive with that of the highest performance cobaltite-based perovskite cathodes. Although stabilized bismuth oxides are attractive materials because of their high oxygen-ion conductivity their phase stability and structural stability are quite complicated and still a subject of controversy.¹⁵⁻¹⁷ Pure bismuth oxide will transform from the high-temperature cubic phase to the monoclinic phase with cooling to $<730^\circ\text{C}$, resulting in a discontinuous drop in conductivity.¹⁸ However, doping strategies involving rare earth elements eliminate the phase transition while maintaining conductivity.

LSM ($\text{La}_{0.8}\text{Sr}_{0.2}\text{MnO}_{3-\delta}$) as a perovskite structure oxide has been widely used as solid oxide fuel cell (SOFC) cathode. It has high catalytic activity for oxygen reduction reaction and very good long term stability.¹⁹⁻²¹ Jiang et al.^{22,23} have reported nanoscale bismuth oxide impregnated LSM electrode for intermediate-temperature SOFCs. At 600°C , the interfacial polarization resistance under open-circuit conditions for electrodes impregnated with 50% bismuth oxide is only 1.3% of the original value for a pure LSM electrode. In addition, as reported in several literature studies^{8,24} bismuth oxide is easy to react with oxides containing cobalt. Therefore, LSM is the best choice for electrode material in bismuth oxide electrolyte based oxygen pump.

In this work, we used dysprosium and tungsten co-doped bismuth (DWSB)²⁵ as electrolyte and DWSB-LSM²³ as electrode to fabricate an oxygen ion conducting ceramic membranes. We prepared DWSB electrolyte with high ionic conductivity at intermediate temperatures while exhibiting chemical compatibility with LSM electrode materials.

^zE-mail: ksbrink@clemson.edu

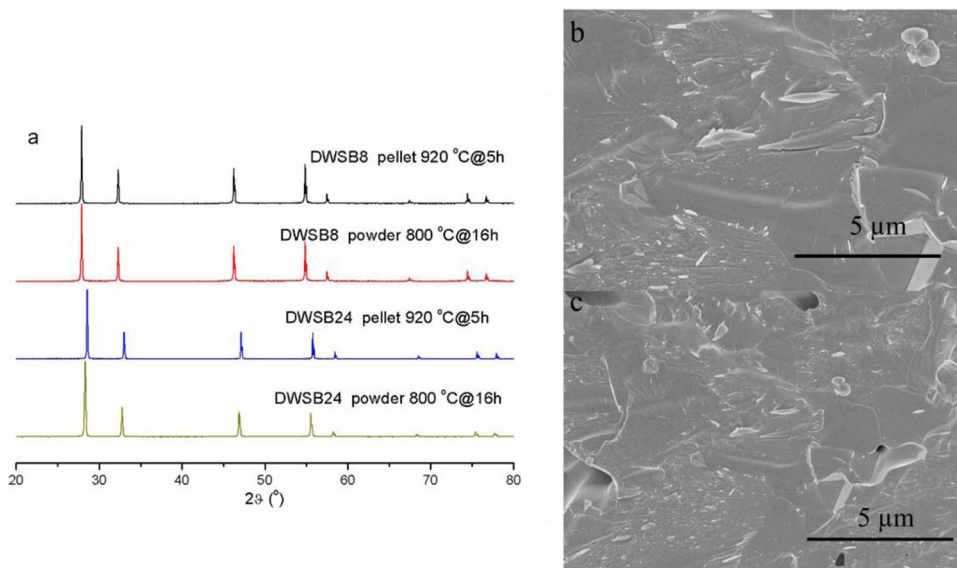


Figure 1. (a) The XRD spectra for DWSB powder and pellet and (b-c) the SEM images for DWSB pellet cross section.

In the DWSB electrolyte supported device with DWSB-LSM as an electrode, the oxygen current density was 1.75 A cm^{-2} under 1 V bias and oxygen flux was $5.4 \text{ mL cm}^{-2} \text{ min}^{-1}$ at 650°C . Further improvement of the electrochemical performance was achieved by employing a thin electrode supported DWSB membrane ($\sim 12 \mu\text{m}$).

Experimental

Powder preparation.—DWSB8 ($\text{Dy}_{0.08}\text{W}_{0.04}\text{Bi}_{0.88}\text{O}_{1.56}$) and DWSB24 ($\text{Dy}_{0.24}\text{W}_{0.08}\text{Bi}_{0.70}\text{O}_{1.5}$) were synthesized by a solid state reaction method. Stoichiometric amounts of the precursors Bi_2O_3 , Dy_2O_3 , and WO_3 (99.5% Alfa Aesar Co. Ltd) were mixed and ball-milled with zirconia ball media in a high-density polyethylene bottle for 24 h. The powders were pressed uniaxially into a disk-shaped 15 mm diameter die using 40 MPa to obtain disk-shaped pellets. The pellets were subsequently sintered in air at 800°C for 16 h to form DWSB with single fluorite structure. The calcined powders were then ground, pressed into a pellet at 200 MPa, and sintered at 930°C for 5 h in air to form dense DWSB samples.

Membrane fabrication.—To evaluate the interfacial polarization resistance, symmetric cells with DWSB-LSM ($(\text{La}_{0.8}\text{Sr}_{0.2})_{0.95}\text{MnO}_{3-\delta}$, Fuelcell Materials Company Co. Ltd) electrode was fabricated on both sides of the DWSB electrolytes. The DWSB-LSM slurry was prepared by mixing the DWSB and LSM powders with an organic binder. The as-prepared slurry was printed onto both sides of the DWSB pellets. After drying under an infrared lamp, the structure was heated at 850°C for 2 h. The electrochemical performance was also characterized with an electrode-supported membrane consisting of a DWSB-LSM electrode supported DWSB thin film electrolyte. To fabricate the electrode-supported membrane, a DWSB-LSM electrode ($\sim 800 \mu\text{m}$) was first fabricated and calcined at 800°C for 2 h. The DWSB electrolyte layer ($\sim 12 \mu\text{m}$) was sequentially deposited on the electrode supported by a particle suspension coating process, followed by sintering at 930°C for 5 h. The other side DWSB-LSM electrode was then applied using the same procedures employed for the fabrication of symmetric cells as described above.

Characterization of phase composition and microstructure of cathodes.—X-ray diffraction (Rigaku TTR-III) analysis was used to examine the phase purity of the DWSB powders as well as the chemical compatibility between DWSB and LSM. The microstructure and morphology of the DWSB pellet and DWSB-LSM electrode were

examined using a scanning electron microscope (SEM) and energy dispersive spectrometer (EDS) (Hitachi S-4800 and S-6600).

Electrochemical measurement.—The electrochemical performance of cathodes was measured using the symmetric cells configuration with Ag as the current collector. Impedance spectra were acquired using a Solartron 1260 electrochemical workstation with an AC amplitude of 10 mV in the frequency range from 1 MHz to 0.1 Hz. The frequency response analyzer was used in standalone mode for unbiased testing and interfaced to a computer using Zplot software. The oxygen permeation flux was studied in a home-built oxygen permeation setup. A permeation cell was constructed by sealing the membranes to an alumina tube using glass powder (Schott D263, Germany) at 700°C for 1 h. The effective area of the membranes for oxygen permeation was 0.35 cm^2 . Oxygen permeation tests were performed at elevated temperatures ($550\text{--}650^\circ\text{C}$) by sweeping helium on the permeate side. The flow rate of inlet gases was controlled by digital mass flowmeter (Alicat Scientific Inc., USA). A gas chromatograph (INFICON Fusion Micro GC) was employed to analyze the composition of the gas mixture. The working voltage was powered by Solartron 1260 electrochemical workstation through silver wire. The oxygen permeation flux was calculated from the oxygen concentration and flow rate of the effluent, and corrected for the oxygen leakage by measuring the nitrogen concentration in the effluent.

Results and Discussion

DWSB powder.—Figure 1a shows the XRD spectra of DWSB powder derived from the solid state reaction. In the doping ratio of 0.08 and 0.24 Dy_2O_3 , both stabilized bismuth oxides have the fluorite structure. We confirmed this structure by powder XRD. The lattice parameter of DWSB8 and DWSB24 is 5.567 \AA and 5.504 \AA , respectively, that was determined from the XRD patterns.²⁵ The lattice parameter decreased with increased Dy concentration due to differences in the ionic radius of the dopant; Dy^{3+} radii were smaller than the Bi^{3+} radii (1.027 and 1.17 \AA in eight coordination, respectively).²⁵ The cross-section SEM images are also shown in Figure 1b that are in good agreement with the literature.¹⁸ The density of the DWSB pellets is about 95% determined by Archimedes method and exhibited the same XRD pattern as the calcined powder.

DWSB conductivity and electrochemical performance.—Figure 2 shows the ionic conductivity of DWSB determined by AC impedance

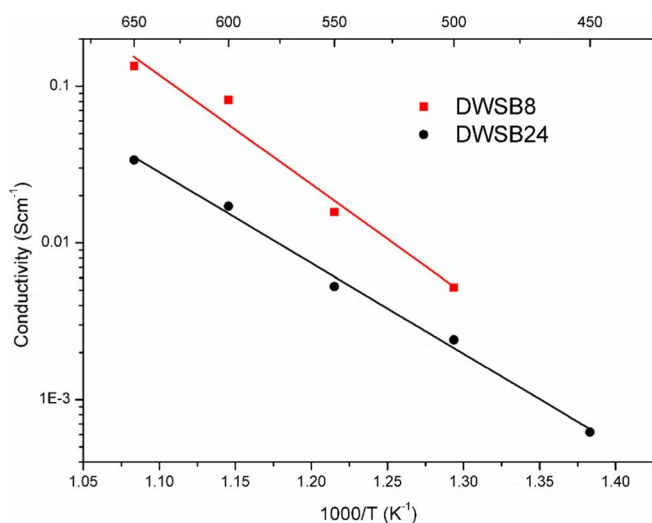


Figure 2. The Arrhenius plots for DWSB8 and DWSB24 electrolyte ionic conductivity determined by AC impedance spectra at 450–650°C.

spectra. The DWSB8 exhibited higher conductivity than DWSB24 over the entire temperature regime from 450–650°C. The conductivity at 650°C was 0.13 and 0.032 Scm^{-1} for DWSB8 and DWSB24, respectively indicating a fourfold increase in conductivity for the DWSB8 material. However, as the temperature decreased, the relative difference became smaller. At 500°C, the conductivity was 0.005 and 0.0022 Scm^{-1} for DWSB8 and DWSB24, respectively. The conductivity of DWSB24 was lower than that of $\text{Dy}_{0.25}\text{W}_{0.05}\text{Bi}_{0.7}\text{O}_{1.56}$ (0.0068 Scm^{-1} at 500°C),¹⁷ but overall the conductivity levels are close. The discrepancy may originate from the slight difference in composition or fabrication process. In the following work, DWSB8 was chosen for the electrolyte material and is subsequently denoted as simply DWSB.

DWSB-LSM electrodes were fabricated in weight fractions of 50:50, 60:40 and 70:30, respectively. Figure 3 gives the SEM images for DWSB-LSM electrode cross-section. It can be seen that the adherence between the dense DWSB electrolyte and the porous DWSB-LSM electrode is very good as revealed in Figures 3a–3b. In the DWSB-LSM composite electrode, the DWSB particle size

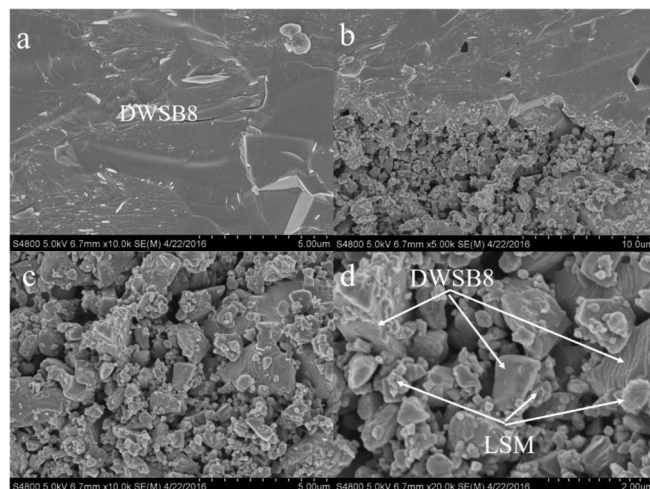


Figure 3. The SEM images for DWSB-LSM electrode cross-section: (a) DWSB electrolyte, (b) interface between DWSB electrolyte and DWSB-LSM electrode, (c) DWSB-LSM electrode and (d) detail image for DWSB and LSM particles.

was larger than that of LSM particle. This is due to the difference in sintering activity of these materials. LSM has a much higher sintering temperature than that of DWSB (~1400 and ~900°C, respectively). Figure 3d indicates the distribution of DWSB and LSM particles. In the composite electrode, larger DWSB particles act as backbone for the oxygen transport pathway, while LSM particles deposited on the surface of the backbone serve as mixed ionic-electronic and oxygen ion conductors accelerating surface oxygen exchange.

The ASR values of DWSB-LSM electrode at 650°C were 0.34, 0.8 and 1.04 Ωcm^2 at weight fraction of 50:50, 60:40 and 70:30 respectively, as shown in Figure 4a. From this result, it could be confirmed that DWSB-LSM composite electrode at the weight fraction of 50:50 demonstrated the best performance. Therefore, in the following work, all the DWSB-LSM composite electrode tests were based on weight fraction 50:50. The ASR values were found to be 0.34, 1.01, 3.15 and 10.6 Ωcm^2 at 650–500°C. The corresponding cathode ASR of DWSB-LSM was quite low (e.g., 1.0 Ωcm^2 at 600°C), drastically reducing

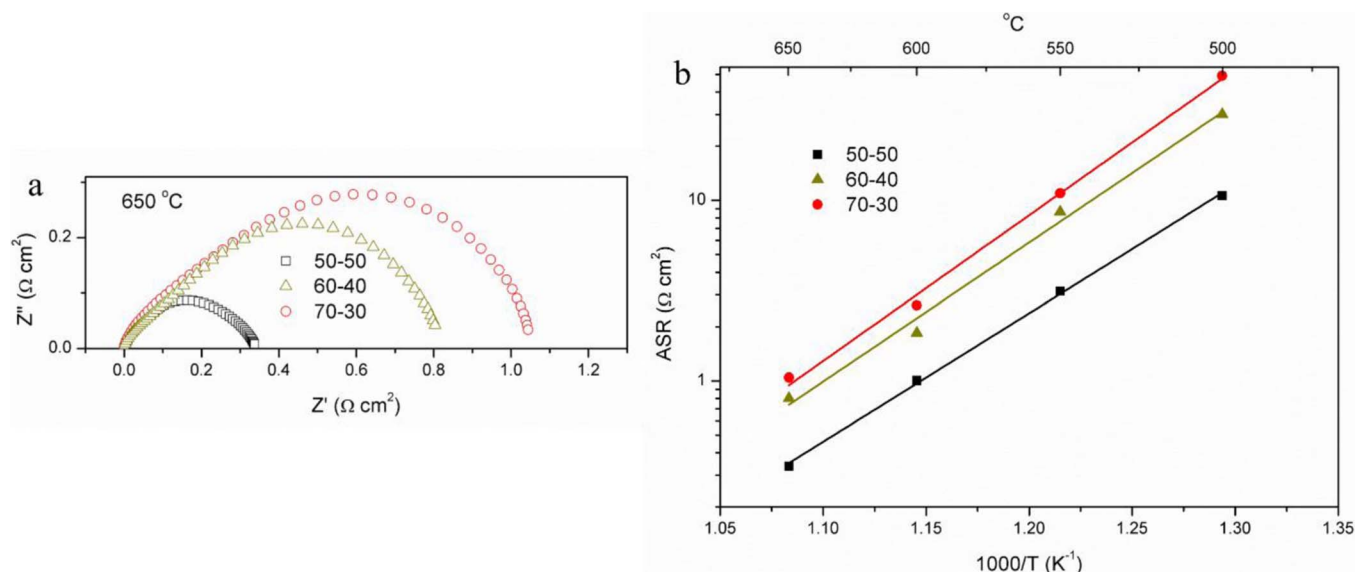


Figure 4. (a) The impedance spectra for DWSB-LSM electrode with different weight fraction at 650°C, and (b) the area specific resistance for DWSB-LSM electrode at the temperature range of 500–650°C.

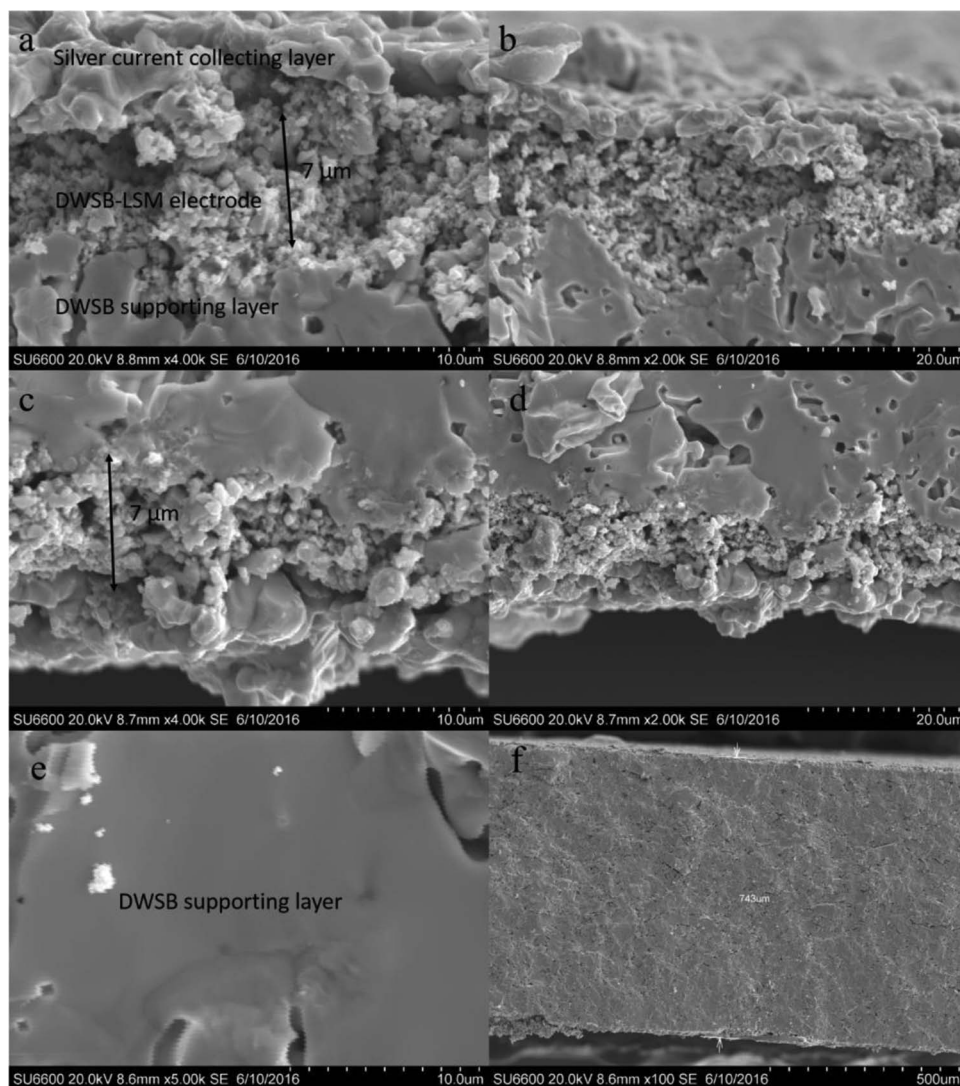


Figure 5. The morphology of DWSB electrolyte supported device. (a-b) cross-section of DWSB-LSM electrode on one side, (c-d) DWSB-LSM electrode on the other side and (e-f) the cross morphology of DWSB supporting layer.

ASR by more than 11 times compared to conventional LSM–YSZ cathodes (e.g., $11.37 \Omega\text{cm}^2$ at 600°C). This result clearly demonstrates the success of the heterostructured cathode design, where the enhanced dissociative adsorption of oxygen occurred on isolated LSM surface while fast oxygen incorporation occurred in the DWSB lattice.

Oxygen permeation performance of DWSB electrolyte supported device.—Figure 5 gives the morphology of DWSB electrolyte supported device with DWSB-LSM electrode on both the feed and permeate sides. The thickness of DWSB-LSM electrode was about $7 \mu\text{m}$, and exhibited good contact with the DWSB electrolyte. The thickness of DWSB electrolyte layer was 0.75 mm (Figure 5f) which was sufficient to provide mechanical strength. The oxygen permeation performance of thick DWSB electrolyte supported device was investigated by the combined electrochemical and gas chromatography setup. In this device, the total resistance was $1.18 \Omega\text{cm}^2$ at 650°C , which increased to 3.2 and $10.3 \Omega\text{cm}^2$ at 600 and 550°C , respectively, Figure 6a. From the IV curve in Figure 6b, we can find that at 650°C , the current deviates from a linear relationship with the applied voltage exhibiting a large increase after 0.9 V . This behavior may be caused by diffusion limitations or electrode activation processes. It was also found that the current density would gradually decrease with elapsed time. At 650°C , the initial current density was 1.75 Acm^{-2} , but after 1 h, it decreased to 1.46 Acm^{-2} or 83% of the original value. In these

conditions with a large current density, the resulting thermal effects may result in the observed performance degradation.

Figure 7a is the schematic diagram of oxygen permeation test device. Under test condition, the oxygen permeation flux of the DWSB electrolyte supported device between 550 and 650°C under 1 V bias is shown in Figure 7b. It is $5.9 \text{ mL min}^{-1}\text{cm}^{-2}$ at 650°C , decreasing to 2.4 and $0.87 \text{ mL min}^{-1}\text{cm}^{-2}$ at 600 and 550°C . In theory, the oxygen permeation flux is expected to increase with increasing operating temperatures due to the increase of DWSB electrolyte oxygen ionic conductivity as well as lower polarization resistance of DWSB-LSM electrode with increasing operating temperature.

The microstructure and chemical composition of the DWSB pump after oxygen permeation flux measurements is shown in Figure 8. The SEM image of the cathode side (Figure 8a) indicates a stable structure was maintained. There was no de-lamination observed between the DWSB-LSM cathode and the DWSB electrolyte. A map of Bismuth (Bi), as a representative element for the DWSB electrolyte (Figure 8c) was homogenous, demonstrating the phase stability of the DWSB electrolyte. While the DWSB-LSM cathode is expected to be an issue in such cathodic working condition, the La mapping image (Figure 8d) suggests a stable cathode morphology after operation. The DWSB-LSM anode microstructure and chemical analysis are also displayed in Figures 8e–8h which confirm stable phase and morphology after cell operation.

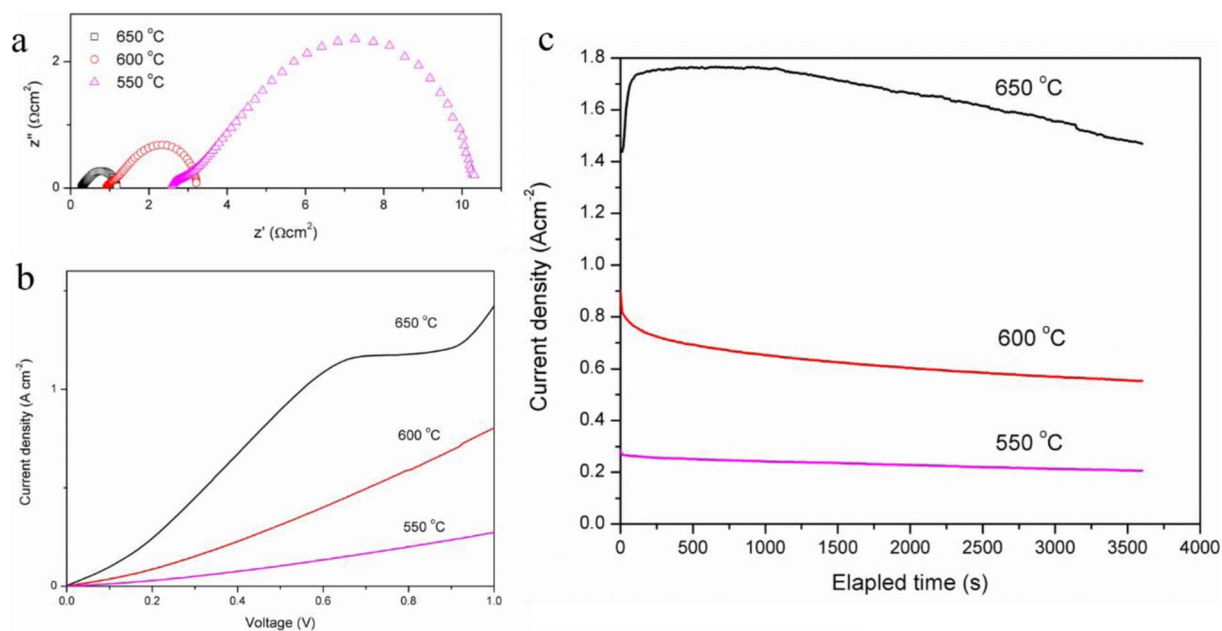


Figure 6. The electrochemical performance of DWSB electrolyte supported oxygen transport membrane at 550–650°C: (a) impedance spectra, (b) the CV curve and impedance spectra of DWSB electrolyte supported device, and (c) the current performance under 1 V voltage with elapsed time.

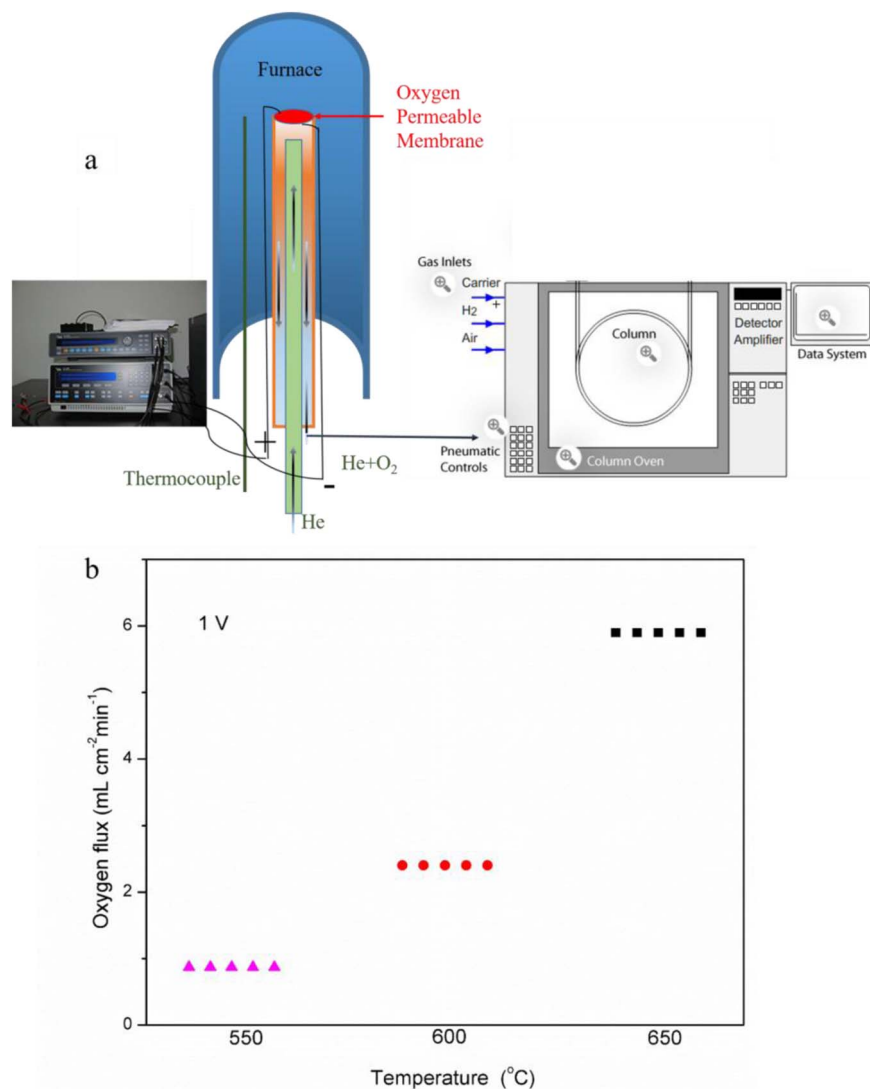


Figure 7. (a) The schematic diagram of oxygen permeation test device and (b) the oxygen flux under 1 V voltage at the temperature range of 550–650°C.

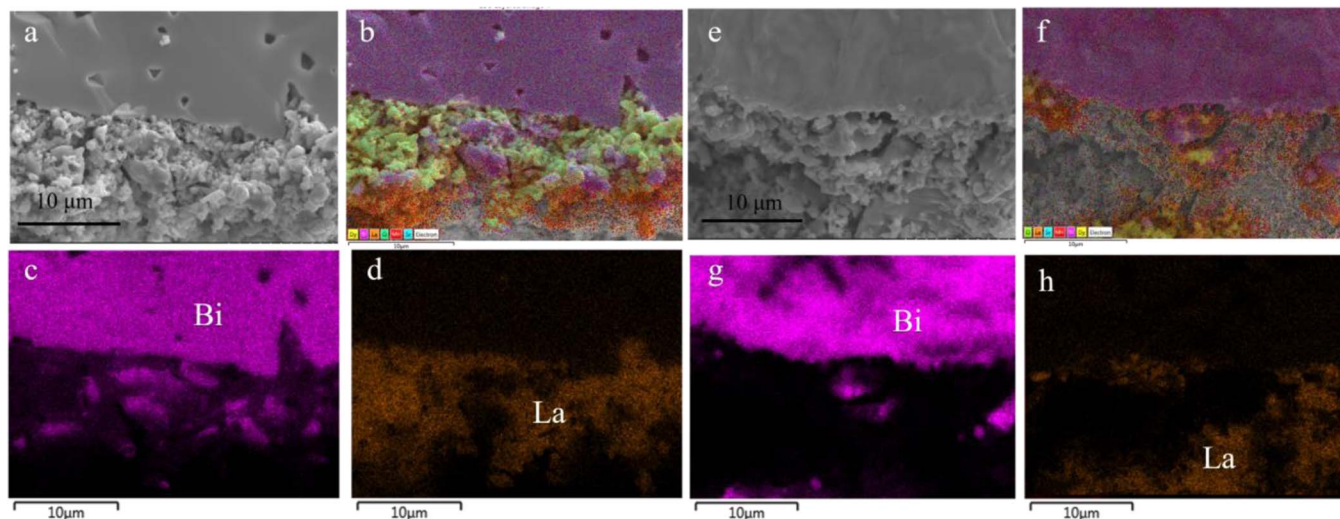


Figure 8. SEM-EDS mapping images of DWSB-LSM cathode (a) SEM image of cross-section, (b) EDS layered image of elements, (c) and (d) Bi and La element EDS mapping, and (e-h) the corresponding images of the DWSB-LSM anode.

IV curve for DWSB-LSM electrode supported DWSB thin film.

As mentioned above, oxygen flux $J = \frac{I}{4F} = \frac{V}{(R_{Ohmic} + R_{pol})4F} = \frac{V}{(\frac{L_{elec}}{\sigma_{elec}} + R_{pol})4F}$, where I is the current, F the Faradays constant, V is the applied voltage, R_{pol} is the electrode polarization resistance, L_{elec} is the electrolyte thickness and σ_{elec} is the electrolyte conductivity. From this equation, we could find that smaller electrolyte thickness could reduce Ohmic resistance, thus improving oxygen flux value. Consequently, in the following experiment, we fabricated a DWSB-LSM electrode supported DWSB thin film membrane. The morphology of the DWSB-LSM electrode supported DWSB electrolyte for thin film electrolyte is shown in Figure 9. Although the DWSB thin layer is not entirely dense, the partially dense DWSB electrolyte was 12 μm thick and strongly connected with the DWSB-LSM electrode, Figure 9b. In this condition, the oxygen permeation flux could not be measured due to leakage associated with insufficient density. However, based on thin film oxygen transport membrane, the electrochemical performance was used to calculate the potential for improved oxygen flux with an electrode supported membrane structure.

The total resistance of thin film device was 0.92, 1.93 and 2.53 Ωcm^2 at 650, 600 and 550°C respectively, Figure 10b. The Ohmic resistance of DWSB electrolyte was 0.44, 1.3 and 1.86 Ωcm^2 respectively. The contribution of the resistance from the electrolyte and electrode is shown in Figure 10c. It could be found that the contribution of electrolyte increased from 73.5% to 47.8% when temperature increased from 550°C to 650°C. This is due to the increased activation energy of the DWSB electrolyte as compared with the DWSB-LSM electrode. The relationship between applied voltage and current is not linear.²⁶ At 650°C, the current density under 2 V was 5 Acm^{-2} which

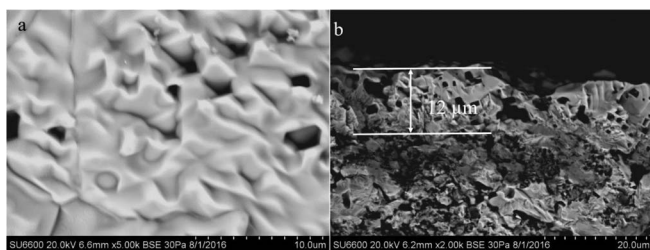


Figure 9. The SEM images for DWSB-LSM electrode supported DWSB thin film electrolyte: (a) DWSB electrolyte surface and (b) DWSB-LSM electrode cross-section with 12 μm thick electrolyte.

is almost 3 times larger than the current with 1 V applied bias as in Figure 10d. This could be due to the smaller polarization resistance of DWSB-LSM electrode at higher voltages.

In our experiment at 650°C and 2 V voltage, the calculated oxygen flux under DWSB thin film electrolyte is about 17 $\text{mL cm}^{-2} \text{min}^{-1}$, which is quite high compared to conventional YSZ based oxygen pump. Although oxygen flux could not be measured due to the partially densified electrolyte, this provides a good estimate. A better densified electrolyte could result in smaller Ohmic resistance and better contact between electrolyte and electrode resulting in a further reduction in the polarization resistance. Further experiments will be focused on processing in order to achieve thin dense electrolytes.

Conclusions

An oxygen transport membrane based on dysprosium and tungsten co-doped bismuth oxide (DWSB) was prepared and characterized. DWSB oxygen ion conducting membrane with the composition of $\text{Dy}_{0.08}\text{W}_{0.04}\text{Bi}_{0.88}\text{O}_{2.8}$ demonstrated the highest ionic conductivity. The weight ratio of DWSB-LSM composite electrode was optimized to 50:50 that has the lowest polarization resistance on DWSB electrolyte. In this composite electrode, larger DWSB particles act as backbone to provide an oxygen transport pathway and LSM particles are deposited on this backbone. In the DWSB electrolyte (0.75 mm) supported membrane with DWSB-LSM electrode on both sides, oxygen flux value of 5.9 $\text{mL cm}^{-2} \text{min}^{-1}$ was obtained at 650°C under 1 V voltage. Further improvements to the electrochemical performance were achieved by fabricating a thin, electrode supported DWSB membrane (~12 μm). The current density for the electrode supported cell was 5.4 Acm^{-2} under 2 V applied bias at 650°C which corresponds to an oxygen flux of 17 $\text{mL cm}^{-2} \text{min}^{-1}$. Higher bias voltages were observed to accelerate the electrode reaction process leading to reduced polarization resistance that resulted in a remarkable growth of current density. This work demonstrates that this intelligent DWSB based oxygen transport membrane is promising for excellent electrochemical performance that can be applied in oxygen separation.

Acknowledgments

We gratefully acknowledge support by the U.S. Army Research Office with SBIR Phase-I award W911NF-16-P-0019. The content of the information does not necessarily reflect the position or the policy of the Government, and no official endorsement should be inferred. Dr. Robert Mantz from the Army Research Labs is gratefully acknowledged for technical discussions.

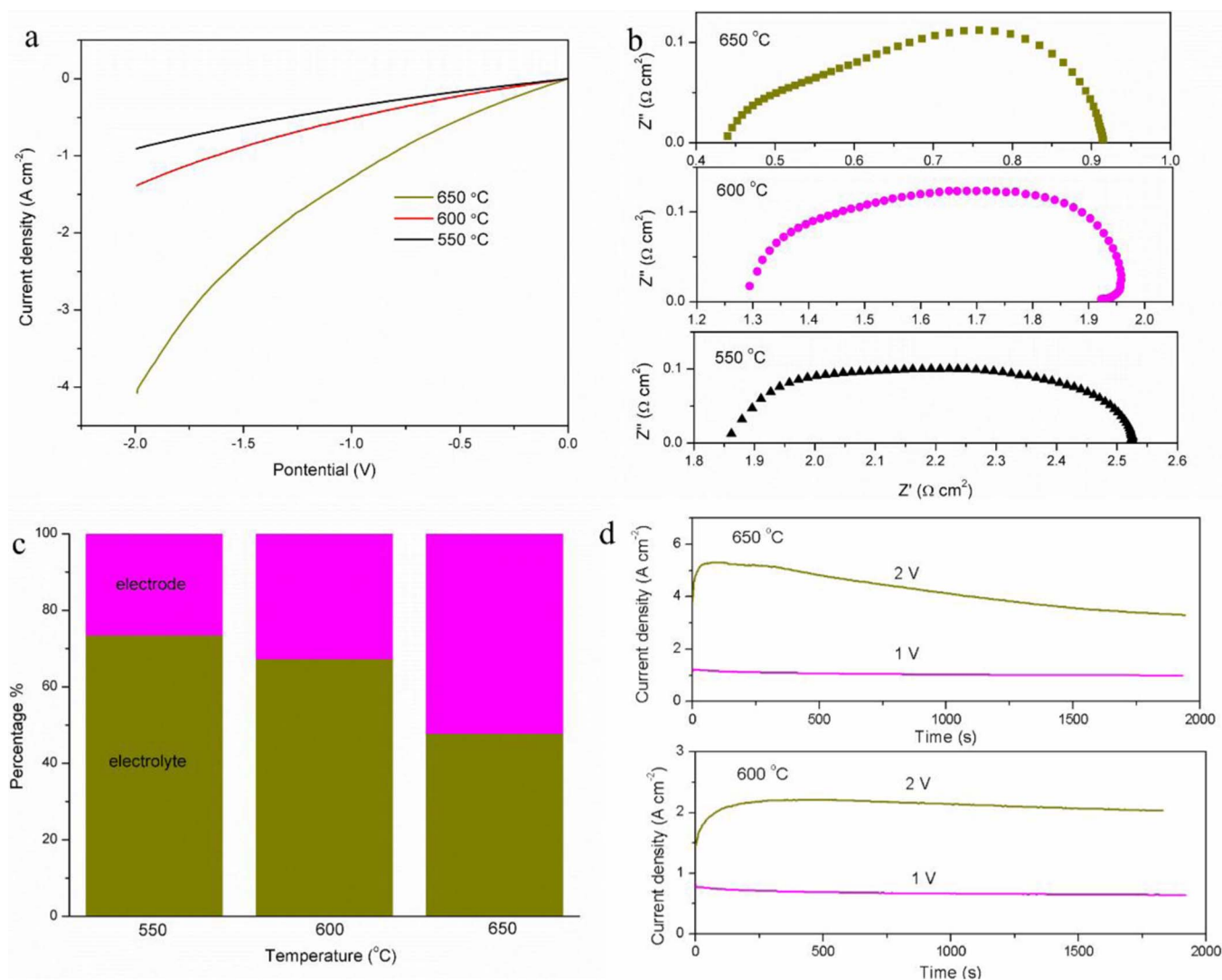


Figure 10. (a) CV curves and (b) impedance spectra for DWSB thin film device at 550–650 °C. (c) The percentage of electrolyte Ohmic resistance and electrode polarization resistance in whole performance and (d) current density change with time under applied voltage at 650 and 600 °C.

References

1. D. Yuan and F. Kröger, *Journal of the Electrochemical Society*, **116**, 594 (1969).
2. P. N. Dyer, R. E. Richards, S. L. Russek, and D. M. Taylor, *Solid State Ionics*, **134**, 21 (2000).
3. K. Brinkman and K. Huang, *Chemical Engineering Progress*, **112**, 44 (2016).
4. T. Liu, Y. Chen, S. Fang, L. Lei, Y. Wang, C. Ren, and F. Chen, *Journal of Membrane Science*, **520**, 354 (2016).
5. T. Hibino, K. Ushiki, and Y. Kuwahara, *Solid State Ionics*, **93**, 309 (1997).
6. A. Spirin, A. Nikonov, A. Lipilin, S. Paragin, V. Ivanov, V. Khrustov, A. Valentsev, and V. Krutikov, *Russian Journal of Electrochemistry*, **47**, 569 (2011).
7. S. Sarat, N. Sammes, and A. Smirnova, *Journal of power sources*, **160**, 892 (2006).
8. E. D. Wachsman and K. T. Lee, *Science*, **334**, 935 (2011).
9. I. Vinke, K. Seshan, B. Boukamp, K. De Vries, and A. Burggraaf, *Solid State Ionics*, **34**, 235 (1989).
10. Y. Zeng and Y. Lin, *Applied Catalysis A: General*, **159**, 101 (1997).
11. N. Jiang and E. D. Wachsman, *Journal of the American Ceramic Society*, **82**, 3057 (1999).
12. Y. Zeng and Y. Lin, *Journal of Catalysis*, **193**, 58 (2000).
13. T. Takahashi, H. Iwahara, and Y. Nagai, *Journal of Applied Electrochemistry*, **2**, 97 (1972).
14. T. Takahashi and H. Iwahara, *Journal of Applied Electrochemistry*, **3**, 65 (1973).
15. S. Boyapati, E. D. Wachsman, and N. Jiang, *Solid State Ionics*, **140**, 149 (2001).
16. V. Fruth, M. Popa, D. Berger, R. Ramer, M. Gartner, A. Ciulei, and M. Zaharescu, *Journal of the European Ceramic Society*, **25**, 2171 (2005).
17. D. W. Jung, K. L. Duncan, M. A. Camaratta, K. T. Lee, J. C. Nino, and E. D. Wachsman, *Journal of the American Ceramic Society*, **93**, 1384 (2010).
18. D. W. Jung, J. C. Nino, K. L. Duncan, S. R. Bishop, and E. D. Wachsman, *Ionics*, **16**, 97 (2010).
19. S. Jiang, Y. Leng, S. Chan, and K. Khor, *Electrochemical and solid-state letters*, **6**, A67 (2003).
20. S. Jiang, J. Love, J. Zhang, M. Hoang, Y. Ramprakash, A. Hughes, and S. Badwal, *Solid State Ionics*, **121**, 1 (1999).
21. X. Xu, Z. Jiang, X. Fan, and C. Xia, *Solid State Ionics*, **177**, 2113 (2006).
22. Z. Jiang, L. Zhang, K. Feng, and C. Xia, *Journal of power sources*, **185**, 40 (2008).
23. Z. Jiang, L. Zhang, L. Cai, and C. Xia, *Electrochimica Acta*, **54**, 3059 (2009).
24. M. Camaratta and E. Wachsman, *Journal of the Electrochemical Society*, **155**, B135 (2008).
25. D. W. Jung, K. L. Duncan, and E. D. Wachsman, *Acta Materialia*, **58**, 355 (2010).
26. Y. Liang, Y. Li, H. Wang, J. Zhou, J. Wang, T. Regier, and H. Dai, *Nature materials*, **10**, 780 (2011).